# Terahertz-Induced Energy Transfer from Hot Carriers to Trions in a MoSe2 Monolayer

Venanzi, T.; Selig, M.; Winnerl, S.; Pashkin, A.; Knorr, A.; Helm, M.; Schneider, H.;

Originally published:

September 2021

**ACS Photonics 8(2021), 2931-2939**

DOI: https://doi.org/10.1021/acsphotonics.1c00394

# Terahertz induced energy transfer from hot carriers to trions in a $MoSe_2$ monolayer

Tommaso Venanzi,[*,†,§] Malte Selig,[‡] Stephan Winnerl,[†] Alexej Pashkin,[†] Andreas Knorr,[‡] Manfred Helm,[†,¶] and Harald Schneider[*,†]

†*Helmholtz-Zentrum Dresden-Rossendorf, 01314 Dresden, Germany*

‡*Institut für Theoretische Physik, Nichtlineare Optik und Quantenelektronik, Technische Universität Berlin, 10623 Berlin, Germany*

¶*Technische Universität Dresden, 01062 Dresden, Germany*

§*Dipartimento di Fisica, Università di Roma "Sapienza", 00185 Rome, Italy*

E-mail: tommaso.venanzi@uniroma1.it; h.schneider@hzdr.de

**Abstract**

Interaction of terahertz (THz) radiation with van der Waals semiconductors represents a considerable interest for optoelectronic applications. Here we report a redshift (around 1 meV) of the trion resonance in $MoSe_2$ monolayer induced by picosecond THz pulses. As its origin, we identify the kinetic excess energy gained by hot carriers due to absorption of THz light which is transferred during the formation of trions. By performing time resolved measurements, we have determined the electron cooling time ($\tau$ = 70 ps) and estimated the absorption at 7.7 THz ($\alpha$ = 0.3%). A quantitative model based on the Heisenberg equation of motion explains the experimental observations and can reproduce the data with good accuracy. The present work gives important insights for the understanding of the trions in van der Waals semiconductors and their interaction with the hot electrons driven by THz radiation.

**Keywords:** Transition metal dichalcogenide monolayers, free electron laser, pump-probe, 2D materials, infrared.

# Introduction

Van der Waals (vdW) semiconductors possess unique properties making them particularly attractive for terahertz/infrared technology. Due to a weak interlayer bonding atomically thin vdW layers can be easily fabricated. The nanoscale thickness of such naturally-formed transition metal dichalcogenide (TMD) quantum wells results in a quantization of electronic energies: mid-infrared intersubband transitions have been observed in $WSe_2$ using a nano-imaging technique.[1] Similar results were obtained in few-layer InSe flakes.[2–4] Furthermore, a coherent modulation of the optical absorption of $MoS_2$ monolayer using intense THz pulses has been demonstrated, showing the feasibility to use TMD monolayer as THz modulators and switches.[5]

On top of these results, the capability to engineer vdW heterostructures greatly expands the possible ways to make vdW semiconductors operating as active materials for terahertz applications.[6–9] For example, infrared interlayer exciton emission has been observed in $WSe_2/MoS_2$ and $InSe/WS_2$ heterostructures.[10,11] However, besides some pioneering works, the research on the THz properties of TMD monolayers did not proceed swiftly so far.[12–17]

One of the important questions that has not been addressed so far is the influence of a THz-induced hot electron distribution on sharp trion and exciton resonances in the near-infrared / visible range. Understanding of this process can facilitate a precise and ultrafast optical read-out of electron temperature in vdW semiconductors that potentially can be utilized for a sensitive THz detection. In this work we study the influence of THz radiation on the optical properties of $MoSe_2$ monolayers by performing THz-pump NIR-probe measurements with the use of the free-electron laser (FEL) FELBE. This unique THz-FEL source allows us to get direct information on the THz response of the materials under in-

vestigation. The THz pulse does not induce interband transitions but mainly leads to a heating of the free carriers in the monolayer, the NIR probe pulse provides information of the induced carrier dynamics via shifts of the exciton and trion resonance. Our experiment monitors the electron dynamics, in the absence of holes, in the conduction band and provides complementary information compared to VIS-pump VIS-probe and to VIS-pump THz-probe experiments.[18–24]

We observe a pronounced redshift of the trion resonance induced by the THz radiation, while the exciton resonance remains almost unperturbed. The trion redshift is mostly due to the energy stored in the background hot carriers after THz absorption. The kinetic energy of hot electrons is transferred during the trion formation, leading to a redshift of the optical transition. A quantitative treatment based on the Heisenberg equation of motion reproduces the experimental observation with good accuracy providing a solid understanding of the observed phenomenon. The model considers the single-particle view of the trion. This description holds in the limit of low electron density, i.e. $E_F \sim 4$ meV$\ll E_B^T$ where $E_F$ is the Fermi energy and $E_B^T$ is the trion binding energy.[25]

The present work gives significant information for the understanding of trion physics in transition metal dichalcogenide monolayers[25–29] and, beyond that, the studied THz properties can be used for broadband infrared detection and other THz technologies.

# Results

The technical details of the THz-pump optical-probe experiment and of the $MoSe_2$ monolayer sample fabrication are described in the experimental methods section.

Figure 1a shows the differential spectra at the time overlap of the pump and probe pulses in comparison with the linear reflectivity at 8 K. The zero-crossing points of the dispersive shapes of the differential signals are located at the trion and exciton energies. Figure 1b shows the evolution in time of the differential reflection spectrum. The FEL excitation

frequency is 7.7 THz (32 meV), far below any electronic transition and not in resonance with the infrared-active phonons.[30,31] The FEL pulse length is 5.5 ps (FWHM) and the fluence is $\phi_{FEL} = 5\ \frac{\mu J}{cm^2}$. The NIR narrowband probe is tuned across the exciton and trion resonances in order to measure the changes in reflection induced by the THz pump as a function of photon energy. We stress that the NIR pulse is only a weak probe of the microscopic polarization. This is proven by the linear dependence of the differential reflection signal with increasing probe fluence (see Supporting Information (SI)[32]) and by the fact that we observe pump-probe NIR signal at the trion energy after the time-overlap of THz and NIR pulses.

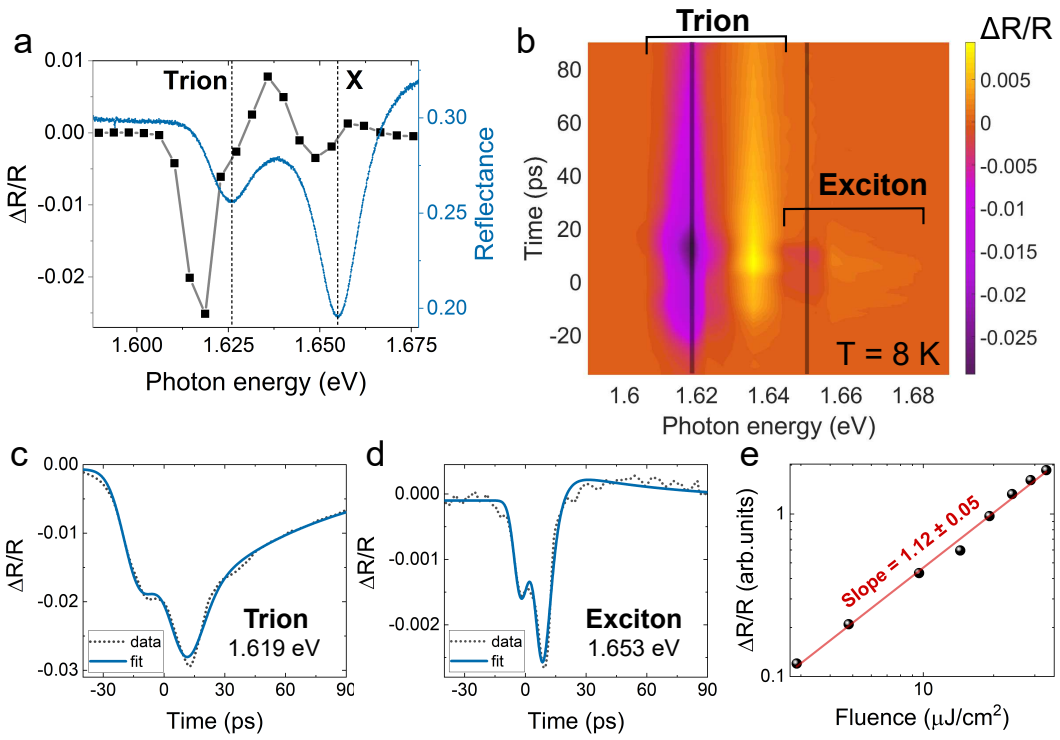


Figure 1: (a) Differential reflection spectra at the time overlap in comparison with the linear reflectivity. The dispersive shapes of the differential signal are located at the trion and exciton energies. (b) Differential reflection spectra in time at $T = 8$ K. A strong and long-living feature is observed at the trion energy. At the exciton energy a fast and weak signal is also observed. (c) and (d) Differential reflection decays at 1.619 eV and 1.653 eV probe energies, i.e. at the trion and the exciton energy, respectively. These two energies are marked in figure 1b. The fast component is limited by the convolution of the pump and probe pulses. The slow component is observable only at trion resonance and has a decay constant of $\tau_2 = 70 \pm 10$ ps. (e) Fluence dependence of the differential signal at the trion energy (1.619 eV).

A strong signal at the trion energy dominates the differential reflection spectrum. Although the exciton provides the prominent signature in the linear spectrum, its signal in the differential reflection is weak. The dispersive shape of the differential reflection signal indicates a redshift of the two resonances induced by the THz radiation. Furthermore, the time trace of the signal at the trion energy shows a slow component that is not observed at the exciton energy.

The time dependence of the differential reflection is shown in Figure 1c and Figure 1d for two specific photon energies corresponding to the trion and exciton resonances, respectively. The weak signal at the exciton energy shows an instantaneous decay, i.e. the decay constant is equal to the time resolution of the setup. Furthermore, the time trace shows two pump pulse replicas. This is due to the reflection at the back side of the substrate. The temporal distance between the two pulses is around 15 ps which corresponds to a distance of $d = \frac{c\,\Delta t}{n_{Si}} = 1.3$ mm, about twice the substrate thickness. Pump pulse replica is a common issue for infrared spectroscopy.[33]

In order to get the time constants of the decays, the differential reflection signals in time were fitted with the convolution of a bi-exponential decay and a response function. The response function is assumed to be Gaussian since is the convolution of the pump and probe laser pulses. The signal at the trion energy shows a bi-exponential decay (Figure 1c). The slow component at the trion resonance has a decay of $\tau_2 = 70 \pm 10$ ps. The fast component is shorter than the time resolution i.e. $t^{fast}_{X,Trion} \leq 6$ ps. To avoid misunderstandings, we note that these time constants have nothing to do with trion or exciton lifetime, rather they characterize the decay dynamics of the THz-induced changes in the trion and exciton resonances.

Similar results were obtained performing the experiment with different FEL photon energies of 14 meV and 24 meV (see SI[32]). This indicates that the differential reflection signal originates from non-resonant absorption of the THz radiation. For this reason, we rule out resonant effects - like transition from trion bound state to continuum or THz excitation of

optical phonons - as possible responsible for the observed signal.[34] The experiment was also repeated on different samples in order to verify the reproducibility of the experiment (see SI,[32] Figure 3). We also note that we did not observe any significant dependence on the linear polarization of the THz radiation with respect to the NIR radiation (data in SI[32]).

The differential signal at a fixed probe photon energy shows a linear dependence on pump power (Figure 1e).

In order to obtain the trion and exciton energy shifts, we fitted the experimental pump-probe data with the difference of two Lorentzian functions for each resonance. The evolution in time of exciton and trion energy shifts are shown in figure 2a. The maximum trion redshift is around $\Delta E_T = 1.1$ meV at FEL fluence of $\phi_{FEL} = 5\ \frac{\mu J}{cm^2}$. Figure 2b shows the differential oscillator strength ($\frac{\Delta I}{I} = \frac{I_{FEL} - I_{noFEL}}{I_{noFEL}}$) as a function of time. The oscillator strength of the trion resonance increases slightly after the arrival of the THz pulse. This indicates that the THz pulse increases slightly the carrier density.

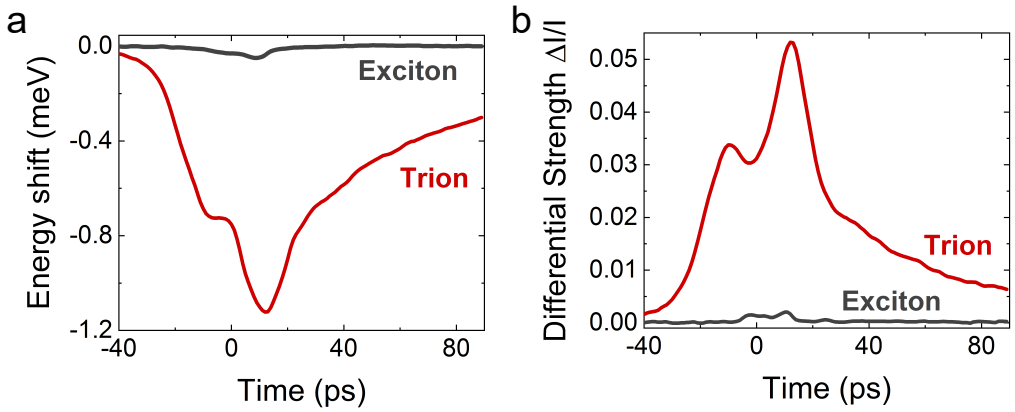


Figure 2: (a) and (b) Time dependence of the energy shift and the differential oscillator strength of the trion and exciton resonances. The values were obtained by fitting the pump-probe spectra with a difference of two Lorentzian functions.

# Discussion

We explain the experimental observations considering THz free-carrier absorption and defect-state absorption. After p erforming the calculation, we find that the dominant effect resp on-

sible for the trion redshift is the energy transfer from hot electrons to trions during the trion formation. We note that also other effects of THz free carrier absorption are included in the mo del, e.g. screening effects and band-gap renormalization.

We will first discuss qualitatively the effect of electron-to-trion energy transfer. Secondly, we discuss qualitatively ~~interpretation of the data and we discuss~~ other p ossible effects of THz radiation which are not included in the mo del and why they were ruled out. Afterwards, we will present the theoretical model and the comparison with the experimental results.

The $MoSe_2$ monolayer has a certain unintentional doping. For this reason, the trion resonance is observed in the NIR reflection spectrum (Fig. 1a). For negative pump-probe delays, i.e. the NIR probe pulse arrives before the THz pump pulse on the sample, no signal is observed. For positive pump-probe delays, the THz pulse causes a heating of the free electrons due to the free carrier absorption, which results in a broadening of the electron momentum distribution. We stress that for positive delays the THz pulse arrives on the sample before the NIR pulse, i.e. when no trions are present in the sample. When the NIR probe pulse arrives on the sample, it creates trions with hot electrons. During the trion formation process, the electron momentum is directly transferred to the center of mass momentum of the trion because of momentum conservation. At the same time, the energy must be conserved: a photon with energy $\hbar\omega$ and an electron with energy $\frac{\hbar^2\mathbf{q}^2}{2m_e}$, where $m_e$ is the electron mass and $\mathbf{q}$ is the momentum, create a trion with energy $E^T + \frac{\hbar^2\mathbf{q}^2}{2M_T}$ that includes trion resting energy $E_T$ and and the kinetic energy $\frac{\hbar^2\mathbf{q}^2}{2M_T}$, where $\mathbf{q}$ and $M_T$ are the momentum and the trion mass, respectively. We note that the electron and the trion momentum must be the same because of momentum conservation. While the trion is heavier than the electron, i.e. $M_T > m_e$, the kinetic energy of the electron is larger compared to the kinetic energy of the center of mass motion of the trion and, consequently, the required photon energy $\hbar\omega$ to form the trion is smaller than $E^T$, which results in a red shift in the spectrum with respect to $E^T$. In fact, the trion optical transition energy is $\hbar\omega = E^T + \frac{\hbar^2\mathbf{q}^2}{2M_T} - \frac{\hbar^2\mathbf{q}^2}{2m_e} \equiv E^T - W_{\mathbf{q}}$.[35] The quantitative treatment of this phenomenon is described in more detail in the theoretical

section.

To visualize this effect, we sketched the mechanism in figure 3.

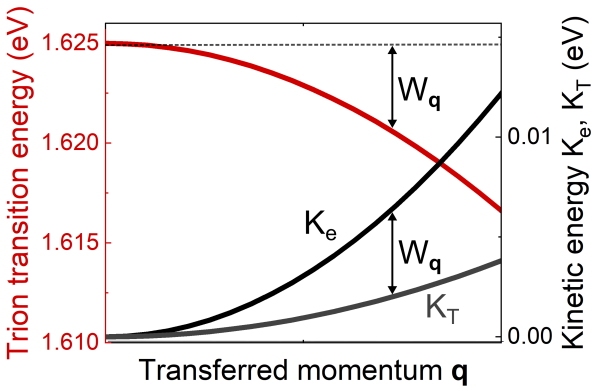


Figure 3: Sketch of the trion optical transition with resp ect to the transferred momentum from the electrons to the trions. On the right axis, there is the kinetic energy of electrons and trions (black and dark grey lines, resp ectively).

Now, we discuss other possible effects of the THz radiation on the $MoSe_2$ monolayer. First of all, we notice that the pump-probe signal is not due to heating of the monolayer lattice via FEL absorption or via substrate heating - inducing Varshni and Polaron shifts of the exciton and trion resonances[36,37] - for two reasons: 1) heating of the lattice would not explain why the signal at the trion energy is around one order of magnitude higher than the signal at the exciton energy; 2) the differential signals at the exciton and at the trion energies would be expected to have the same time constants. To get a more quantitative proof, we have measured the dependence of the trion and exciton energies on the lattice temperature (see SI[32]), showing that the trion and the exciton resonances undergo similar redshift with increasing lattice temperature. This is not compatible with our pump-probe data.

THz radiation can induced a transient change of the refractive index of the substrate. This effect was also ruled out since it cannot explain the slow component of the signal observed at the trion energy. For the same reason, ac Stark, dynamical Franz-Keldysh, and field ionization effects have to be ruled out as well[17,38] (see SI for more details[32]).

Free-carrier absorption and defect-state absorption give an explanation for the redshift of the trion peak, while leaving the exciton peak almost unperturbed. The following theoretical

description supports this interpretation providing good agreement with the experimental observations.

## Theoretical model

The quantitative description of these phenomena was obtained following the approach developed by Esser et al. for the calculation of the exciton and trion spectra.[35,39] A detailed summary of the derivation of the trionic and excitonic microscopic polarizations in terms of Green's functions and of the total susceptibility is reported in SI.[32]

The starting point is to find the exciton and trion wavefunctions by solving the eigenvalue problem. The Wannier equation of the exciton reads:[40]

$$\frac{\hbar^2\mathbf{q}^2}{2m}\varphi^{\nu}_{\mathbf{q}} - \sum_{\mathbf{k}} V_{\mathbf{k}}\varphi^{\nu}_{\mathbf{q}-\mathbf{k}} = E_B^{X\nu}\varphi^{\nu}_{\mathbf{q}}, \tag{1}$$

with the Fourier component of the excitonic relative motion $\mathbf{q}$, the reduced mass of the exciton $m$ and the Coulomb potential $V_{\mathbf{q}}$, which is obtained from *ab initio* calculations.[41] The solution of the Wannier equation gives access to excitonic wave functions $\varphi^{\nu}_{\mathbf{q}}$ and binding energies $E_B^{X\nu}$ for the exciton state $\nu$.

The Schrödinger equation of the trion reads

$$\left(\frac{\hbar^2(\mathbf{q_1}^2+\mathbf{q_2}^2)}{2m} + \frac{\hbar^2\mathbf{q_1}\cdot\mathbf{q_2}}{2m_h}\right)\Psi^{\mu}_{\mathbf{q_1},\mathbf{q_2}} + \sum_{\mathbf{k}} V_{\mathbf{k}}\left(\Psi^{\mu}_{\mathbf{q_1}+\mathbf{k},\mathbf{q_2}-\mathbf{k}} - \Psi^{\mu}_{\mathbf{q_1}-\mathbf{k},\mathbf{q_2}} - \Psi^{\mu}_{\mathbf{q_1},\mathbf{q_2}-\mathbf{k}}\right) = E_B^{T\mu}\Psi^{\mu}_{\mathbf{q_1},\mathbf{q_2}}, \tag{2}$$

with the Fourier components of the of the motion of both electrons relative to the hole $\mathbf{q_{1/2}}$, the reduced mass of the electron hole pair $m$, hole mass $m_h$, trion wave function $\Psi^{\mu}_{\mathbf{q_1},\mathbf{q_2}}$ and binding energy $E_B^{T\mu}$ for the trion state $\mu$.

The Wannier equation, eq. 1, and the trion Schrödinger equation, eq. 2, are solved with a Ritz variational ansatz.[42] The trial wavefunctions are reported in SI.[32]

The linear optical susceptibility is given as

$$\chi^{\sigma}(\omega) = \frac{e}{\epsilon_0 \omega^2 m_0 \Omega A_0^{\sigma}(\omega)} \sum_{\mathbf{k},s} M_{\mathbf{k}}^{vc\sigma} P_{\mathbf{k}}^{s}(\omega), \tag{3}$$

with the elementary charge $e$, the free electron mass $m_0$, the vacuum permittivity $\epsilon_0$, $A_0^{\sigma}$ is the vector potential of the incident light field, $M_{\mathbf{k}}^{vc\sigma}$ are the optical matrix elements, $\Omega$ is the sample area, and light polarization $\sigma$. By exploiting Heisenberg equation of motion we calculate the Bloch equations for the excitonic polarization $P^{\lambda,s} = \sum_{\mathbf{k}} \varphi_{\mathbf{k}}^{*\lambda} \langle c_{\mathbf{k}}^{\dagger s} d_{-\mathbf{k}}^{\dagger -s} \rangle$ with electron and hole annihilation (creation) operators $c_{\mathbf{k}}^{(\dagger)s}/d_{\mathbf{k}}^{(\dagger)-s}$ with momentum $\mathbf{k}$ and spin $s$. Via Coulomb interaction it couples to the trion polarization $T_{\mathbf{q}}^{\mu s_1 s_2} = \sum_{\mathbf{k_1},\mathbf{k_2}} \Psi_{\mathbf{k_1},\mathbf{k_2}}^{\mu} \langle c_{\mathbf{k_1}+\frac{m_e}{M_T}\mathbf{q}}^{\dagger s_1} c_{\mathbf{k_1}+\frac{m_e}{M_T}\mathbf{q}}^{\dagger s_1} d_{\frac{m_h}{M_T}\mathbf{q}-\mathbf{k_1}-\mathbf{k_2}}^{\dagger s_1} c_{\mathbf{q}}^{s_2} \rangle$ for which we also derive an equation of motion by exploiting the Heisenberg equation. The upcoming hierarchy problem is truncated by omitting 6-operator quantities.[35] The resulting system of equations is solved via Fourier transformation.

We note that in the calculation of the optical susceptibility of the trion we fo cus on terms app earing in linear order of the electron o ccupation, b eing valid at weak doping. Consequently, our mo del do es not capture effects which arise in higher orders of the doping density which are for instance renormalizations of the trion energy $E^T$ or screening effects.[43]

Focusing on the lowest lying exciton and trion states, we access an expression for the linear susceptibility:

$$\chi(\omega) = \chi_0 \Big( \frac{\left| L^X \right|^2}{E^X + \delta E - \hbar\omega - i\gamma^X} + \frac{1}{\Omega} \sum_{\mathbf{q}} f_{\mathbf{q}} \frac{\left| L_{\mathbf{q}}^T \right|^2}{E^T - W_{\mathbf{q}} - \hbar\omega - i\gamma^T} \Big). \tag{4}$$

The first term accounts for the exciton resonance, where $L^X = \frac{1}{\Omega} \sum_{\mathbf{q}} \varphi_{\mathbf{q}} (1 - f_{\mathbf{q}}^e)$ is the excitonic coupling strength, the electron occupation is treated in thermal approximation, i.e. $f_{\mathbf{q}}^e = \left( \exp\left( \frac{\frac{\hbar^2 \mathbf{q}^2}{2m_e} - E_F(n,T)}{k_B T} \right) + 1 \right)^{-1}$ is the Fermi-Dirac distribution where $E_F(n,T)$ is the Fermi level, $E^X = E^g + E_B^X$ is the excitonic transition energy which is given by the band gap $E^g$ and the binding energy of the exciton $E_B^X$. $\gamma^X$ is introduced to account for the homogeneous

broadening of the exciton.[36,37,44,45] The Hartree-Fock term $\delta E$ is given by[40]

$$\delta E = \frac{1}{\Omega^2} \sum_{\mathbf{k},\mathbf{q}} \varphi_{\mathbf{k}} V_{\mathbf{q}} (f^e_{\mathbf{k}} \varphi_{\mathbf{k}-\mathbf{q}} - f^e_{\mathbf{k}-\mathbf{q}} \varphi_{\mathbf{k}}) \tag{5}$$

with the 2D screened Coulomb potential $V_{\mathbf{q}}$.[41,46,47] The two addends in equation (5) are the reduction of the exciton binding energy (blueshift) and the reduction of the band gap (redshift) due to the presence of carriers in the conduction band. With the Coulomb potential used in our calculation (see SI[32]), an increase of the carrier temperature induces a decrease of this term and, therefore, leads to a redshift of the exciton energy. Conversely, an increase of carrier density induces a blueshift of the exciton resonance. Since the increase of carrier temperature and carrier density are linked to each other, the two effects partially compensate.

The second term in equation 4 accounts for the optical response of the trion. It is given as a sum of Lorentzian oscillators weighted with the electron occupation $f^e_{\mathbf{q}}$ with coupling strength $L^T_{\mathbf{q}} = \frac{1}{\Omega} \sum_{\mathbf{k}} \Psi_{\mathbf{q},\mathbf{k}}$ reflecting that each doping electron with momentum $\mathbf{q}$ contributes to the formation of a trion with center of mass momentum $\mathbf{q}$. The optical transition energy of each oscillator is given as $E^T - W_{\mathbf{q}}$ where the first term $E^T = E^g + E^T_B$ includes the band gap and the trion binding energy $E^T_B$.[35] The kinetic energy transfer $W_{\mathbf{q}} = \frac{\hbar^2 \mathbf{q}^2}{2m_e} - \frac{\hbar^2 \mathbf{q}^2}{2M_T} = \frac{\hbar^2 \mathbf{q}^2 M_X}{2m_e M_T}$, where $M_X$ is the exciton mass, originates from the energy and momentum conservation during the trion formation process as we discussed above. $\gamma^T$ is introduced to take into account an homogeneous broadening of the exciton and trion resonances.[36,37,44,45]

Figures 4a and 4b show the dependence of the trion and exciton energies on the carrier temperature and carrier density considering the Hartree-Fock shift and the electron recoil $W_{\mathbf{q}}$. The dependence of the optical transition energies as function of carrier density is in qualitative agreement with previous reports.[26,48–53] The carrier temperature dependence of the trion and exciton resonances is not easily comparable with any previous experiment.

From Equation (4), it is possible to calculate the reflection spectra $R(\omega)$ (details in SI[32]). Figure 4c shows the experimental and calculated spectra of the $MoSe_2$ monolayer at

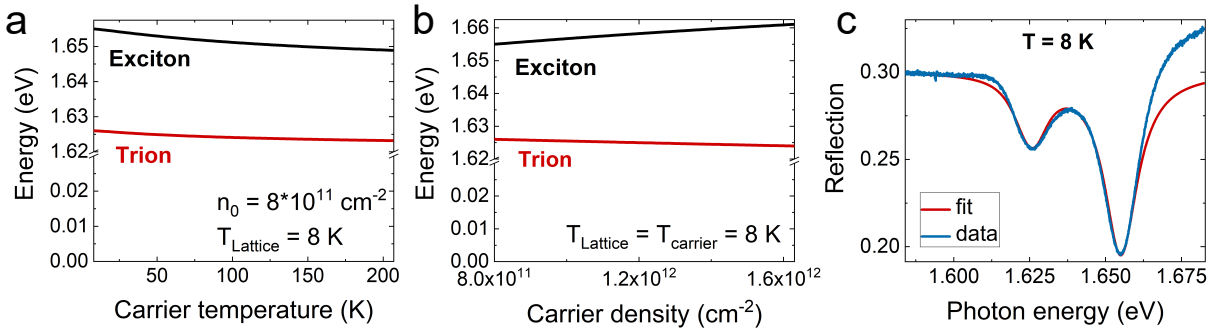


Figure 4: (a) and (b) Trion and exciton energies as a function of carrier temperature and carrier density, respectively. The Hartree-Fock shift in equation 5 and the electron recoil $W_{\mathbf{q}}$ are considered. (c) Measured reflection spectrum of $MoSe_2$ monolayer at $T = 8$ K (blue curve) and calculated spectrum (red curve) based on equation 4.

$T = 8$ K. The carrier density is adjusted to match the relative oscillator strength of exciton and trion and is determined to be $n_e = 8.5 \cdot 10^{11}$ cm$^{-2}$. This value indicates a significant intrinsic doping of the monolayer[47,48,50] which is due to laser-doping effects from the pulsed NIR probe laser.[54,55] Therefore, the monolayer is supposedly negatively charged.[56] For this reason, we restricted the discussion to the negative trion, neglecting the presence of free holes in the monolayer.

Assuming a quasi-thermal equilibrium of the carriers at any delay time, the time evolution of the pump-probe signal can be reproduced as differential reflection using the carrier temperature $T_c$ and the carrier density $n_e$ as parameters:

$$\frac{\Delta R}{R}(\omega, t) = \frac{\Delta R}{R}(\omega, T_c, n_e) = \frac{R(\omega, T_c, n_e) - R(\omega, T_0, n_0)}{R(\omega, T_0, n_0)} \tag{6}$$

where $R(\omega, T)$ is obtained as described above. We attribute the change in carrier temperature and density to free carrier absorption, defect-state absorption and impact ionization by hot carriers.

## Theoretical results

Figures 5a and 5b show the comparison between experimental data and the results of the theory presented above. Figure 5a shows the calculated differential spectrum signal at the time overlap of pump and probe pulses, and figure 5b shows the calculated time dependence at the trion energy (1.619 eV). The theory is in good agreement with the experimental observations, pointing towards the fact that the proposed model includes the main physical contributions that lead to observed data. The details of the fitting procedure are explained thoroughly in SI.[32] We note here that we used only two free parameters to fit the data, i.e. carrier density and temperature. In any case, there is a small but significant quantitative disagreement between experiment and theory. This is more pronounced at the time overlap of the NIR and FEL pulses (Fig. 5a). Therefore, possible causes of this disagreement are ac-Stark or Franz-Keldysh effect. The non-thermal distribution of the hot electrons could also play a role.

Figures 5c and 5d show the change in carrier temperature and carrier density as a function of time. The maximum change in the carrier temperature is $\Delta T_c = 32$ K and the change of carrier density is around 20% of the initial doping value.

Furthermore, we calculated the full differential reflection signal in time to get a direct comparison with the experimental data in figure 1a. Figure 5e shows the 2D false-color plot of the calculated differential reflection spectra. The calculation based on the model presented above shows a good agreement with the experimental observations.

From the change in the carrier temperature, we estimate the absorption of the THz radiation by the $MoSe_2$ monolayer. Assuming the electron heat capacity $c_v^{2D} = \frac{\pi^2}{3} n_e k_B \frac{k_B T}{E_F}$, the THz absorption is estimated as:

$$\eta_{abs} \simeq \frac{\Delta T_c c_v^{2D} A_{mono}}{E_{pulse}(\frac{d_{mono}}{d_{FEL}})^2} \simeq 3 \cdot 10^{-3}. \tag{7}$$

where $E_{pulse}$ is the pulse energy, $A_{mono}$ is the monolayer area, $d_{mono}$ and $d_{FEL}$ are the flake size

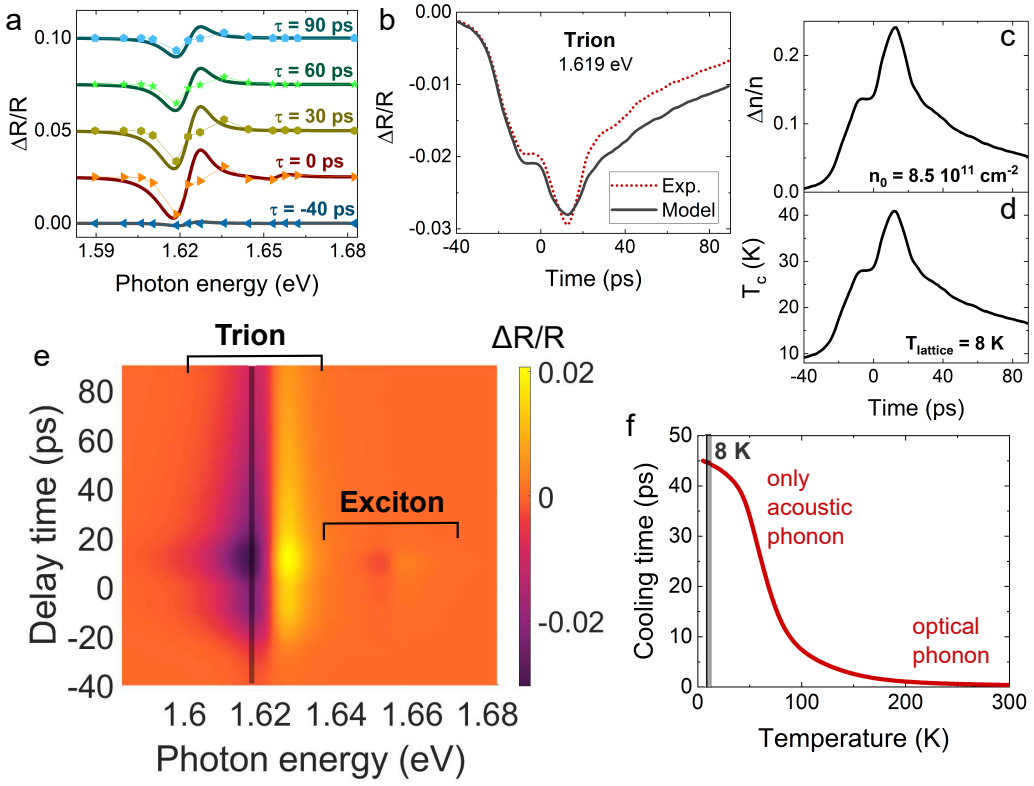


Figure 5: (a) Comparison between the calculated (lines) and measured (dots) differential reflection spectra at different delay time. The curves are shifted vertically for clarity. (b) Comparison between calculated and measured differential reflection decay at the trion energy (1.619 eV, marked in figure 5e). (c) and (d) Carrier density and carrier temperature as a function of delay time, respectively. The slow component of the electron cooling has a decay constant of 70 ps. (e) 2D false-color plot of the calculated differential reflection signal. The carrier temperature and the carrier density were used as fitting parameters. The simulation is in good agreement with experimental data shown in figure 1b. (f) Temperature dependence of the hot electron cooling time. The cooling time increases considerably at low temperatures because it is determined mainly by the less efficient acoustic phonon emission.

and the FEL spot size, respectively. As cross-check, the absorption is calculated with a Drude model. Assuming the electron scattering time of $\tau = 10^{-12}$ s,[57] the absorption coefficient is $\alpha = \frac{ne^2}{\epsilon_0 c m_e \omega^2 \tau} = 1.5 \cdot 10^6$ m$^{-1}$ and the absorption is $a = 1 - e^{-\alpha d} \simeq \alpha d = 0.9 \cdot 10^{-3}$, where $d = 0.6$ nm is the monolayer thickness. The two values of absorption are in good agreement, suggesting that the analysis of the trion redshift in terms of carrier heating is the correct interpretation.

Finally, we theoretically investigate the cooling of free carriers via carrier-phonon scattering in order to explain the long decay time observed in the experiment. By implementing Boltzmann equations that include absorption and emission processes of acoustic and optical phonons, we calculate $\tau_{cooling} = 45$ ps at $T_{lattice} = 8$ K (Fig. 5f). A detailed description of this calculation is reported in SI.[32] The value of the cooling time obtained from the microscopic analysis is similar to the experimental value of 70 ps. The increase of cooling time at low temperatures is due to the optical phonon bottleneck: the optical phonons have too high energy in comparison to the thermal energy of carriers and do not contribute efficiently for the cooling of the electron distribution. The cooling is mainly determined via the less efficient acoustic phonon scattering.

# Conclusion

We have demonstrated that THz radiation induces free carrier and defect-state absorption in $MoSe_2$ monolayers which results in pronounced redshifts of the trion resonance in the transient reflection. While free carriers transfer momentum and energy to the trions leading to a net redshift of trion resonance, defect-state absorption leads to an increase of the carrier density that partially compensates the redshift of the exciton peak. By performing time resolved pump probe experiments, we found that the relaxation time of the free carriers is $\tau = 70$ ps after THz absorption. This value is in agreement with the microscopic calculation of cooling via phonon emission. The absorption at 7.7 THz is estimated to be around 0.3%.

A quantitative model based on the Heisenberg equation of motion theory reproduces the experimental data with good agreement and gives a solid understanding of the phenomenon.

Our study broadens the comprehension of the impact of THz radiation on transition metal dichalcogenide monolayers. More generally, the dynamics of the energy transfer between free carriers and trions was observed for the first time in any semiconductor system. This knowledge is an important step for the development of terahertz technology that uses vdW semiconductors as building blocks.

## Experimental methods

The sample was fabricated via mechanical exfoliation. The substrate is high-resistivity silicon with a 90 nm thin $SiO_2$ layer on top. The sample is placed in a cold finger cryostat and was kept at $T = 8$ K during the measurements.

The pump-probe setup is arranged in a reflection geometry (see SI[32]). As probe beam, a narrowband Titanium:Sapphire (TiSa) oscillator is used. As pump beam, the infrared FEL was used. The infrared spot diameter is around 400 $\mu$m, i.e. much larger than the $MoSe_2$ monolayer flake. However, the NIR probe laser was focused on a spot diameter of 3 $\mu$m. In this way, the signal was collected only from the monolayer flake.

The time resolution is limited by the THz pulse length of $\tau_{FEL} = 5.5$ ps (see SI[32]). The repetition rate of the TiSa laser was reduced from 78 MHz to 13 MHz with a electro-optic pulse-picker in order to match the repetition rate of the FEL. The two sources were synchronized using the electronic signal from the FEL as master clock and a mirror mounted on a piezo for the fine adjustment of the repetition rate of TiSa oscillator.

## Acknowledgement

The authors are grateful to Michael Klopf and the ELBE team for the operation of the free electron laser FELBE. The authors thank Himani Arora, Artur Erbe, and Dominik

Christiansen for fruitful discussions. M.S. gratefully acknowledges funding from the Deutsche Forschungsgemeinschaft through Project No. 432266622 (SE 3098/1).

## Supporting Information Available

Pump-probe data at different THz frequencies, temperature dependent PL spectra, trion theory and details of fitting and calculations.

## References

(1) Schmidt, P.; Vialla, F.; Latini, S.; Massicotte, M.; Tielrooij, K. J.; Mastel, S.; Navickaite, G.; Danovich, M.; Ruiz-T., D. A.; Yelgel, C.; Fal'ko, V.; Thygesen, K. S.; Hillenbrand, R.; Koppens, F. H. Nano-imaging of intersubband transitions in van der Waals quantum wells. Nat. Nanotechnol. **2018**, 13, 1035–1041.

(2) Magorrian, S. J.; Ceferino, A.; Zólyomi, V.; Fal'ko, V. I. Hybrid k · p tight-binding model for intersubband optics in atomically thin InSe films. Phys. Rev. B **2018**, 97, 165304.

(3) Zultak, J.; Magorrian, S. J.; Koperski, M.; Garner, A.; Hamer, M. J.; Tóvári, E.; Novoselov, K. S.; Zhukov, A. A.; Zou, Y.; Wilson, N. R.; Haigh, S. J.; Kretinin, A. V.; Fal'ko, V. I.; Gorbachev, R. Ultra-thin van der Waals crystals as semiconductor quantum wells. Nat. Commun. **2020**, 11, 125.

(4) Kudrynskyi, Z. R.; Kerfoot, J.; Mazumder, D.; Greenaway, M. T.; Vdovin, E. E.; Makarovsky, O.; Kovalyuk, Z. D.; Eaves, L.; Beton, P. H.; Patanè, A. Resonant tunnelling into the two-dimensional subbands of InSe layers. Communications Physics **2020**, 3, 16.

(5) Shi, J.; Baldini, E.; Latini, S.; Sato, S. A.; Zhang, Y.; Pein, B. C.; Shen, P.-C.; Kong, J.;

Rubio, A.; Gedik, N.; Nelson, K. A. Room Temperature Terahertz Electroabsorption Modulation by Excitons in Monolayer Transition Metal Dichalcogenides. Nano Lett. **2020**, 20, 5214–5220.

(6) Koppens, F. H. L.; Mueller, T.; Avouris, P.; Ferrari, A. C.; Vitiello, M. S.; Polini, M. Photodetectors based on graphene, other two-dimensional materials and hybrid systems. Nat. Nanotechnol. **2014**, 9, 780–793.

(7) Liu, Y.; Huang, Y.; Duan, X. Van der Waals integration before and beyond two-dimensional materials. Nature **2019**, 567, 323–333.

(8) Long, M.; Wang, P.; Fang, H.; Hu, W. Progress, Challenges, and Opportunities for 2D Material Based Photodetectors. Adv. Funct. Mater. **2019**, 29, 1803807.

(9) Xia, J.; Yan, J.; Wang, Z.; He, Y.; Gong, Y.; Chen, W.; Sum, T. C.; Liu, Z.; Ajayan, P. M.; Shen, Z. Strong coupling and pressure engineering in WSe2–MoSe2 heterobilayers. Nat. Physics **2021**, 17, 92–98.

(10) Karni, O.; Barré, E.; Lau, S. C.; Gillen, R.; Ma, E. Y.; Kim, B.; Watanabe, K.; Taniguchi, T.; Maultzsch, J.; Barmak, K.; Page, R. H.; Heinz, T. F. Infrared Interlayer Exciton Emission in $MoS_2/WSe_2$ Heterostructures. Phys. Rev. Lett. **2019**, 123, 247402.

(11) Ubrig, N. et al. Design of van der Waals interfaces for broad-spectrum optoelectronics. Nat. Mater. **2020**, 19, 299–304.

(12) Sie, E. J.; Lui, C. H.; Lee, Y.; Fu, L.; Kong, J.; Gedik, N. Large, valley-exclusive Bloch-Siegert shift in monolayer $WS_2$. Science **2017**, 355, 1066–1069.

(13) Poellmann, C.; Steinleitner, P.; Leierseder, U.; Nagler, P.; Plechinger, G.; Porer, M.; Bratschitsch, R.; Schüller, C.; Korn, T.; Huber, R. Resonant internal quantum transitions and femtosecond radiative decay of excitons in monolayer $WSe_2$. Nat. Materials **2015**, 14, 889–893.

(14) Merkl, P.; Mooshammer, F.; Steinleitner, P.; Girnghuber, A.; Lin, K.; Nagler, P.; Holler, J.; Schüller, C.; Lupton, J. M.; Korn, T.; Ovesen, S.; Brem, S.; Malic, E.; Huber, R. Ultrafast transition between exciton phases in van der Waals heterostructures. Nat. Mater. **2019**, 26, 25–28.

(15) Langer, F.; Schlauderer, S.; Gmitra, M.; Fabian, J.; Korn, T.; Steiner, J. T.; Kira, M.; Huber, R.; Huttner, U. Lightwave valleytronics in a monolayer of tungsten diselenide. Nature **2018**, 557, 76–80.

(16) Steinleitner, P.; Merkl, P.; Graf, A.; Nagler, P.; Watanabe, K.; Taniguchi, T.; Zipfel, J.; Schüller, C.; Korn, T.; Chernikov, A.; Brem, S.; Selig, M.; Berghäuser, G.; Malic, E.; Huber, R. Dielectric Engineering of Electronic Correlations in a van der Waals Heterostructure. Nano Lett. **2018**, 18, 1402–1409.

(17) Yong, C. K.; Utama, M. I. B.; Ong, C. S.; Cao, T.; Regan1, E. C.; Horng, J.; Shen, Y.; Cai, H.; Watanabe, K.; Taniguchi, T.; Tongay, S.; Deng, H.; Zettl, A.; Louie, S. G.; Wang, F. Valley-dependent exciton fine structure and Autler-Townes doublets from Berry phases in monolayer $MoSe_2$. Nat. Mater. **2019**, 18, 1065.

(18) Kumar, N.; Cui, Q.; Ceballos, F.; He, D.; Wang, Y.; Zhao, H. Exciton-exciton annihilation in MoSe2 monolayers. Phys. Rev. B **2014**, 89, 125427.

(19) Wang, H.; Zhang, C.; Rana, F. Ultrafast dynamics of defect-assisted electron-hole recombination in monolayer $MoS_2$. Nano Lett. **2015**, 15, 339–345.

(20) Schmidt, R.; Berghäuser, G.; Schneider, R.; Selig, M.; Tonndorf, P.; Malić, E.; Knorr, A.; Michaelis De Vasconcellos, S.; Bratschitsch, R. Ultrafast Coulomb-Induced Intervalley Coupling in Atomically Thin WS2. Nano Lett. **2016**, 16, 2945–2950.

(21) Singh, A. et al. Trion formation dynamics in monolayer transition metal dichalcogenides. Phys. Rev. B **2016**, 93, 041401(R).

(22) Robert, C.; Lagarde, D.; Cadiz, F.; Wang, G.; Lassagne, B.; Amand, T.; Balocchi, A.; Renucci, P.; Tongay, S.; Urbaszek, B.; Marie, X. Exciton radiative lifetime in transition metal dichalcogenide monolayers. Phys. Rev. B **2016**, 93, 205423.

(23) Ruppert, C.; Chernikov, A.; Hill, H. M.; Rigosi, A. F.; Heinz, T. F. The Role of Electronic and Phononic Excitation in the Optical Response of Monolayer WS2after Ultrafast Excitation. Nano Lett. **2017**, 17, 644–651.

(24) Lui, C. H.; Frenzel, A. J.; Pilon, D. V.; Lee, Y. H.; Ling, X.; Akselrod, G. M.; Kong, J.; Gedik, N. Trion-induced negative photoconductivity in monolayer $MoS_2$. Physical Review Letters **2014**, 113, 1–5.

(25) Imamoglu, A.; Cotlet, O.; Schmidt, R. Exciton-polarons in two-dimensional semiconductors and the Tavis-Cummings model. arXiv **2020**, 2006.15963v1.

(26) Efimkin, D. K.; MacDonald, A. H. Many-body theory of trion absorption features in two-dimensional semiconductors. Phys. Rev. B **2017**, 95, 035417.

(27) Sidler, M.; Back, P.; Cotlet, O.; Srivastava, A.; Fink, T.; Kroner, M.; Demler, E.; Imamoglu, A. Fermi polaron-polaritons in charge-tunable atomically thin semiconductors. Nat. Physics **2017**, 13, 255–261.

(28) Fey, C.; Schmelcher, P.; Imamoglu, A.; Schmidt, R. Theory of exciton-electron scattering in atomically thin semiconductors. Phys. Rev. B **2020**, 101, 195417.

(29) Tempelaar, R.; Berkelbach, T. C. Many-body simulation of two-dimensional electronic spectroscopy of excitons and trions in monolayer transition metal dichalcogenides. Nat. Commun. **2019**, 10, 1–7.

(30) Sekine, T.; Izumi, M.; Nakashizu, T.; Uchinokura, K.; Matsuura, E. Raman Scattering and Infrared Reflectance in 2H-MoSe2. J. Phys. Soc. Jpn **1980**, 49, 1069–1077.

(31) Tonndorf, P.; Schmidt, R.; P., B.; Zhang, X.; Boerner, J.; Liebig, A.; Albrecht, M.; Kloc, C.; Gordan, O.; Zahn, D. R. T.; Michaelis de Vasconcellos, S.; Bratschitsch, R. Photoluminescence emission and Raman response of monolayer $MoS_2$, $MoSe_2$, and $WSe_2$. Optics Express **2013**, 21, 4908.

(32) See Supplementary Information.

(33) Winnerl, S.; Orlita, M.; Plochocka, P.; Kossacki, P.; Potemski, M.; Winzer, T.; Malic, E.; Knorr, A.; Sprinkle, M.; Berger, C.; de Heer, W. A.; Schneider, H.; Helm, M. Carrier Relaxation in Epitaxial Graphene Photoexcited Near the Dirac Point. Phys. Rev. Lett. **2011**, 107, 237401.

(34) Sarkar, S.; Goswami, S.; Trushin, M.; Saha, S.; Panahandeh-Fard, M.; Prakash, S.; Tan, S. J. R.; Scott, M.; Loh, K. P.; Adam, S.; Mathew, S.; Venkatesan, T. Polaronic Trions at the MoS2/SrTiO3 Interface. Advanced Materials **2019**, 31, 1903569.

(35) Esser, A.; Zimmermann, R.; Runge, E. Theory of Trion Spectra in Semiconductor Nanostructures. Phys. status solidi (b) **2001**, 227, 317–330.

(36) Christiansen, D.; Selig, M.; Berghäuser, G.; Schmidt, R.; Niehues, I.; Schneider, R.; Arora, A.; de Vasconcellos, S. M.; Bratschitsch, R.; Malic, E.; Knorr, A. Phonon Sidebands in Monolayer Transition Metal Dichalcogenides. Phys. Rev. Lett. **2017**, 119, 187402.

(37) Lengers, F.; Kuhn, T.; Reiter, D. E. Phonon-mediated exciton capture in Mo-based transition metal dichalcogenides. Phys. Rev. Research **2020**, 2, 043160.

(38) Keldysh, L. V. The effect of a strong electric field on the optical properties of insulating crystals. J. Exptl. Theoret. Phys. (U.S.S.R.) **1958**, 34, 1138–1141.

(39) Esser, A.; Runge, E.; Zimmermann, R.; Langbein, W. Photoluminescence and radiative lifetime of trions in GaAs quantum wells. Phys. Rev. B **2000**, 62, 8232–8239.

(40) Kira, M.; Koch, S. Many-body correlations and excitonic effects in semiconductor spectroscopy. Progress in Quantum Electronics **2006**, 30, 155 – 296.

(41) Trolle, M. L.; Pedersen, T. G.; Véniard, V. Model dielectric function for 2D semiconductors including substrate screening. Sci. Rep. **2017**, 7, 1–9.

(42) Berkelbach, T. C.; Hybertsen, M. S.; Reichman, D. R. Theory of neutral and charged excitons in monolayer transition metal dichalcogenides. Phys. Rev. B **2013**, 88, 045318.

(43) Verdenhalven, E.; Binder, R.; Knorr, A.; Malić, E. Derivation of the screened Bloch equations and application to carbon nanostructures. Chemical Physics **2013**, 413, 3–10.

(44) Selig, M.; Berghäuser, G.; Raja, A.; Nagler, P.; Schüller, C.; Heinz, T. F.; Korn, T.; Chernikov, A.; Malic, E.; Knorr, A. Excitonic linewidth and coherence lifetime in monolayer transition metal dichalcogenides. Nat. Commun. **2016**, 7.

(45) Katsch, F.; Selig, M.; Knorr, A. Exciton-Scattering-Induced Dephasing in Two-Dimensional Semiconductors. Phys. Rev. Lett. **2020**, 124, 257402.

(46) Chernikov, A.; Berkelbach, T. C.; Hill, H. M.; Rigosi, A.; Li, Y.; Aslan, O. B.; Reichman, D. R.; Hybertsen, M. S.; Heinz, T. F. Exciton binding energy and nonhydrogenic Rydberg series in monolayer $WS_2$. Phys. Rev. Lett. **2014**, 113, 076802.

(47) Florian, M.; Hartmann, M.; Steinhoff, A.; Klein, J.; Holleitner, A. W.; Finley, J. J.; Wehling, T. O.; Kaniber, M.; Gies, C. The Dielectric Impact of Layer Distances on Exciton and Trion Binding Energies in van der Waals Heterostructures. Nano Lett. **2018**, 18, 2725–2732, PMID: 29558797.

(48) Ross, J. S.; Wu, S.; Yu, H.; Ghimire, N. J.; Jones, A. M.; Aivazian, G.; Yan, J.; Mandrus, D. G.; Xiao, D.; Yao, W.; Xu, X. Electrical control of neutral and charged excitons in a monolayer semiconductor. Nat. Commun. **2013**, 4, 1473–1476.

(49) Shepard, G. D.; Ardelean, J. V.; Ajayi, O. A.; Rhodes, D.; Zhu, X.; Hone, J. C.; Strauf, S. Trion-Species-Resolved Quantum Beats in MoSe2. ACS Nano **2017**, 11, 11550–11558.

(50) Mak, K. F.; He, K.; Lee, C.; Lee, G. H.; Hone, J.; Heinz, T. F.; Shan, J. Tightly bound trions in monolayer MoS2. Nat. Mater. **2013**, 12, 207–211.

(51) Lundt, N.; Cherotchenko, E.; Iff, O.; Fan, X.; Shen, Y.; Bigenwald, P.; Kavokin, A. V.; Höfling, S.; Schneider, C. The interplay between excitons and trions in a monolayer of $MoSe_2$. Appl. Phys. Lett. **2018**, 112, 031107.

(52) Goldstein, T.; Wu, Y.-C.; Chen, S.-Y.; Taniguchi, T.; Watanabe, K.; Varga, K.; Yan, J. Ground and excited state exciton polarons in monolayer MoSe 2 . J. Chem. Phys. **2020**, 153, 071101.

(53) Chang, Y. W.; Reichman, D. R. Many-body theory of optical absorption in doped two-dimensional semiconductors. Phys. Rev. B **2019**, 99, 125421.

(54) Cadiz, F. et al. Ultra-low power threshold for laser induced changes in optical properties of 2D molybdenum dichalcogenides. 2D Materials **2016**, 3, 45008.

(55) Venanzi, T.; Arora, H.; Erbe, A.; Pashkin, A.; Winnerl, S.; Helm, M.; Schneider, H. Exciton localization in $MoSe_2$ monolayers induced by adsorbed gas molecules. Appl. Phys. Lett. **2019**, 114, 172106.

(56) Tongay, S.; Zhou, J.; Ataca, C.; Liu, J.; Kang, J. S.; Matthews, T. S.; You, L.; Li, J.; Grossman, J. C.; Wu, J. Broad-range modulation of light emission in two-dimensional semiconductors by molecular physisorption gating. Nano Lett. **2013**, 13, 2831–2836.

(57) Esaki, L.; Tsu, R. Superlattice and Negative Differential Conductivity in Semiconductors. IBM J. Research .Development **1970**, 14, 61–65.

**For Table of Contents Use Only**

**Title:** Terahertz induced energy transfer from hot carriers to trions in a $MoSe_2$ monolayer

**Authors:** Tommaso Venanzi, Malte Selig, Stephan Winnerl, Alexej Pashkin, Andreas Knorr, Manfred Helm, and Harald Schneider

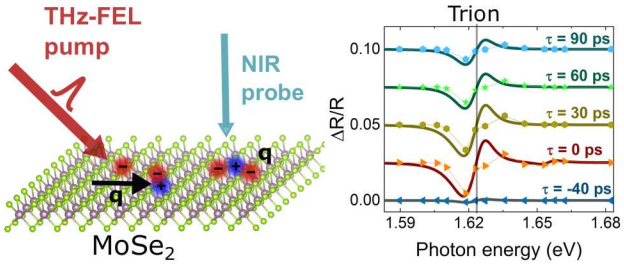


The TOC figure shows on the left a sketch of the mechanism that causes the redshift of the trion resonance. The mechanism is the transfer of energy from the free electrons, heated by the THz pulse, to the trions. The kinetic energy of the trion center mass decreases the energy of the trion optical transition. On the right, there are the differential reflection spectra as function of time. A strong signal at the trion energy is observed and it decreases with a decay constant related to the cooling time of the hot electron distribution.